Nanotechnology 18 (2007) 445304 (6pp) doi:10.1088/0957-4484/18/44/445304

GaP/GaAsP/GaP core–multishell nanowire heterostructures on (111) silicon

P K Mohseni[1], C Maunders[2], G A Botton[2] and R R LaPierre[1,3]

[1] Center for Emerging Device Technologies, Department of Engineering Physics, McMaster University, Hamilton, ON, L8S 4L7, Canada
[2] Canadian Center for Electron Microscopy and Department of Materials Science and Engineering, McMaster University, Hamilton, ON, L8S 4L7, Canada

E-mail: lapierr@mcmaster.ca

Received 23 August 2007, in final form 4 September 2007
Published 9 October 2007
Online at stacks.iop.org/Nano/18/445304

Abstract
GaP/GaAsP/GaP segmented nanowires were grown by gas source molecular beam epitaxy on silicon (111) substrates. The nanowires were grown by the vapour–liquid–solid process using Au nanoparticles. Transmission electron microscopy and energy dispersive x-ray spectroscopy indicated that the wires had wurtzite crystal structure with a core–multishell heterostructure. Stacking faults along the wire were removed after the growth-interrupted interfaces, indicating the potential for defect-free nanowires.

1. Introduction

Over the past decade, one-dimensional nanowires (NWs) have been proven as powerful building blocks in active nanometer-scale devices. Compound semiconductor NWs are particularly attractive for optoelectronic device applications, as demonstrated by NW-based light-emitting diodes (LED) [1], tunable bio-sensors [2], lasers [3], optical waveguides [4], and photonic crystal structures [5].

Carrier confinement in heterostructures provides an opportunity to increase the efficiency of radiative recombination of electrons and holes [6]. As first demonstrated in Si/Ge/Si systems [7], core–multishell NW structures, wherein a material of smaller bandgap is enclosed radially by two layers of a larger bandgap material, would provide realization of the required quantum confinement. Such structures, when appropriately doped, would lend themselves most immediately to p–i–n LED and photodiode applications.

Recently, III–V compound semiconductor NWs have been epitaxially grown on silicon and germanium substrates via chemical vapor deposition (CVD) and molecular beam epitaxy (MBE) [8–12]. Such monolithic integration represents an ideal marriage between III–V optoelectronics and silicon, the well-established backbone of the microelectronics industry. The use of NWs resolves the drawbacks associated with heteroepitaxially deposited films of compound semiconductors on silicon; namely a relatively large mismatch of lattice constants and thermal expansion coefficients. As theoretically shown by Zervos *et al* [13], the strain induced at heterointerfaces in NWs is elastically relieved over a thickness of a few monolayers due to the large NW surface area in comparison to its volume, and small contact area between a NW and its substrate.

In this work, we present the epitaxial growth of core–multishell GaP/GaAsP/GaP NWs on a (111) silicon substrate by gas source molecular beam epitaxy. The growth is attributed to the vapor–liquid–solid (VLS) mechanism [14–16], wherein gold nanoparticles are employed as selective assembly sites for gas-phase adatoms. Upon supersaturation of the semiconductor–metal alloy, nucleation of adatoms occurs at the interface between the Au seed particle and the substrate, localized to the spatial extent of the seed. A continued flux of gas-phase adatoms promotes subsequent growth of one-dimensional semiconductor NWs. We report a core–multishell structure in segmented GaP/GaAsP/GaP NWs due to the interplay between axial growth of the NWs, and deposition on the sidewalls of the NWs.

2. Experimental details

GaP/GaAsP/GaP segmented NWs were grown on Si(111) substrates. The Si(111) substrates were boron-doped at 10^{16} cm^{-3}. The substrates were initially subjected to a 20 min ultraviolet (UV) ozone treatment for growth of a sacrificial oxide layer and removal of surface bonded hydrocarbons. The oxide layer was then etched for 30 s in a diluted 10:1 HF

[3] Author to whom any correspondence should be addressed.

 © 2007 IOP Publishing Ltd Printed in the UK

solution and rinsed in de-ionized water. The etched substrates were transferred in ambient air to an electron-beam evaporation system for the deposition of a 10 Å thick film of Au, as determined by a quartz crystal thickness monitor. The Au-deposited samples were kept under high vacuum (10^{-8} Torr) in the electron-beam evaporation chamber until transport in ambient air to the growth chamber.

The growth was performed in a gas source molecular beam epitaxy (GS-MBE) system wherein group III species (Ga) were supplied as monomers from a heated solid elemental effusion cell while the group V species were supplied as dimers (As_2 or P_2) from a hydride (AsH_3 or PH_3) gas cracker operating at a temperature of 950 °C. Prior to the initiation of the growth, the Au-coated substrate was heated to a growth temperature of 510 °C while being subjected to an inductively coupled hydrogen plasma treatment under a P_2 overpressure. This process allows for the formation of uniformly distributed Au nanoparticles on the Si surface.

The growth was initiated by opening the shutter of the Ga effusion cell, whose temperature was preset to yield a nominal planar growth rate of 1 μm h^{-1}. The first GaP layer was nominally p-doped with Be to 10^{18} cm^{-3}, as determined by prior doping calibrations based on GaAs layers on (100) GaAs substrates. The GaP layer was grown for a duration of 20 min, at which point the Ga and Be shutters were closed for a growth interruption of 3 min. The subsequent layer was grown with an As/P flux ratio corresponding to a nominal composition of $GaAs_{0.6}P_{0.4}$, as determined from previous thin film calibrations on GaAs(100) substrates. The growth of this second layer was terminated after 10 min and this was followed by a growth interruption of 3 min. The final layer, composed of GaP, was nominally n-doped with Si to 10^{18} cm^{-3} as determined by prior doping calibrations (again consisting of GaAs layers on (100) GaAs substrates). Growth of the GaP layer was terminated after 10 min and the substrate cooled down from the growth temperature under a P_2 overpressure. Throughout the growth, the V/III flux ratio was maintained constant at 1.5.

After growth, the orientation, morphology and distribution of the as-grown NWs were studied using a JEOL JSM-7000 scanning electron microscope (SEM) in the secondary-electron mode. NWs were suspended in a small volume of de-ionized water after a 1 min sonication bath and applied to a carbon holey grid in preparation for transmission electron microscopy (TEM). Single NWs were subsequently investigated with a Philips CM12 TEM, a JEOL 2010F for high resolution transmission electron microscopy (HRTEM) and analytical TEM (ATEM), and an FEI Titan 80-300 HB high resolution TEM. This latter instrument is equipped with a sextupole-based aberration corrector of the imaging lens system providing a resolution of 0.75 Å (point resolution and information limit). After tuning the imaging lens system, residual spherical aberrations in the order of 1 μm were achieved. Composition analysis of the radial heterostructures was performed via energy dispersive x-ray spectroscopy (EDXS) in the JEOL 2010F using Kα x-ray transitions.

3. Results and discussion

First, the overall morphology of the NWs was examined by SEM. A cross-sectional SEM image of the NWs on the Si(111) substrate, shown in figure 1, indicated that planar growth on the Si surface between the NWs (the regions not covered by Au) was limited to a thickness of roughly 120 nm. The wires were tapered with an average full width at half-maximum (FWHM) diameter of 52 nm, and an average height of 5.1 μm as measured from the top surface of the two-dimensional film growth. The tapering is predominantly located near the tip of the NW with the remaining portion having a nearly uniform diameter. This tapered structure was previously attributed to a layer-by-layer growth mechanism on the NW sidewalls [17], and will not be discussed in detail here. The use of a 10 Å thick Au film, as opposed to a 40 Å thick film in previous growths [18], resulted in enhanced uniformity in seed size and distribution, leading to more densely packed NWs. The presence of Au nanoparticles at the NW tips, as indicated by EDXS, gave confirmation of the VLS growth mechanism.

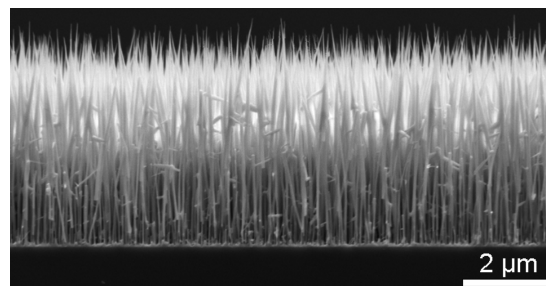

Figure 1. Cross-sectional SEM image of GaP/GaAsP/GaP nanowires as-grown on Si(111).

Next, we examined the composition of the NWs using ATEM. A bright-field HRTEM image and EDXS linescans obtained from a single NW are shown in figure 2. In figure 2(a), results are shown for an EDXS linescan along the axis of the NW (along the growth direction). In addition, a series of linescans were performed across the diameter of the top, middle, and base segments of the NW, labeled 1, 2, and 3, respectively, in figure 2(a). The corresponding EDXS results for the scans along lines 1, 2, and 3 are shown in figures 2(b), (c), and (d), respectively. Green, blue, and red lines correspond to EDXS counts of elemental Ga, P, and As, respectively.

First, we focus on the tip of the NW. The Ga linescan (green line) in figure 2(a) indicates an approximately constant Ga content, as expected for both GaAsP and GaP segments, up to the NW tip where the Ga signal decreases due to the NW tapering. A similar decrease is observed in the P signal (blue line) near the NW tip, while the As signal (red line) is negligible in this region, indicating that the tip of the NW is composed of GaP. The results of the EDXS scan along line 1, shown in figure 2(b), confirm the GaP composition of the wire tip.

Next, we turn our attention to the middle segment of the NW. The linescan along the NW axis in figure 2(a) indicates the presence of both As and P near the middle segment. The results of the EDXS scan along line 2, shown in figure 2(c), indicate that the As count (red line) is greatest in a core region, then vanishes in a sheath region of the NW. Accordingly, the P count (blue line) is greatest in the NW sheath and is somewhat lower in the core region. These results suggest that, in the middle segment of the NW, there exists a GaAsP core surrounded by a GaP shell.

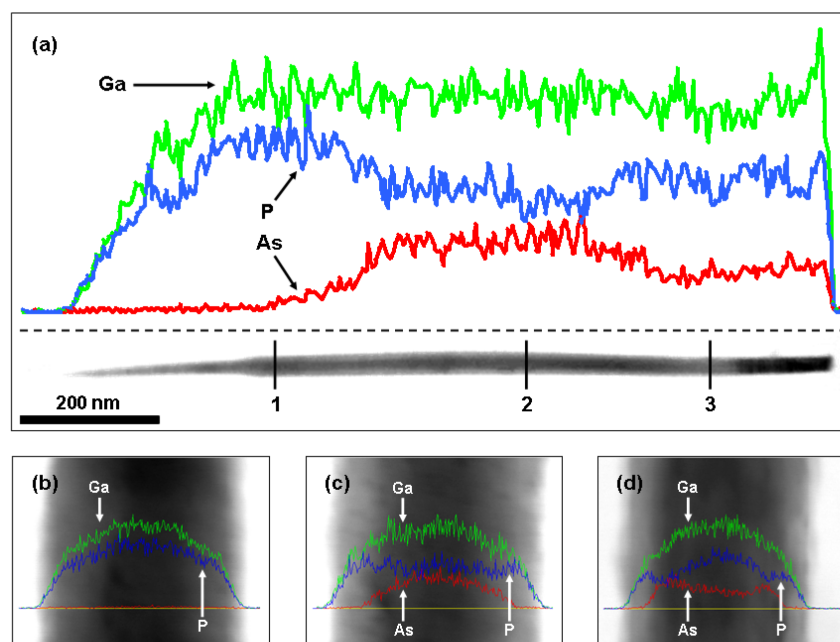

Figure 2. (a) A TEM image and superimposed axial EDXS linescans of a single NW showing variations in Ga (green), P (blue), and As (red) compositions. The dotted line denotes the length of the linescan across the center of the NW. (b) The radial EDXS scan corresponding to line 1 in (a) suggests an outer GaP shell at the NW tip. (c) The radial EDXS scan corresponding to line 2 in (a) shows the presence of a GaAsP layer in the center of the wire with a GaP shell. (d) The radial EDXS scan corresponding to line 3 in (a) indicates that a GaP core is encapsulated by a GaAsP shell, both of which are coated by a secondary shell of GaP.

Finally, we consider the base segment of the NW. The axial linescan in figure 2(a) indicates a P content which is somewhat greater compared to that for the middle segment, and lower compared to that for the NW tip. Correspondingly, the As content in the base is noticeably lower in relation to that for the middle segment and greater in relation to that for the NW tip. The results of the EDXS scan along line 3 of figure 2(a), shown in figure 2(d), indicate a negligible As content along the NW sheath, indicating an outer GaP shell as observed previously for the middle segment of the NW. Moving towards the NW core, the P signal (blue line) is observed to decrease, while the As signal increases, suggesting an inner sheath region of GaAsP, also similar to the earlier results for the NW middle segment. Finally, at the NW core, the P signal (blue line) is maximum, while the As signal (red line) decreases, suggesting a predominantly GaP core composition. Note that As is still detected in the core region at the base of the NW due to the presence of a GaAsP layer, encapsulating the GaP core.

Consideration of the above axial and radial EDXS linescans leads us to conclude that the GaP–GaAsP–GaP segmented growth is best described with the core–multishell arrangement shown conceptually in figure 3. The growth begins with a segment of GaP resulting in the core of the NW (inner shaded region). Axial VLS growth at the Au–wire interface and uncatalyzed radial growth on the NW sidewalls results in a shell of GaAsP, represented by the white region of figure 3. Finally, the growth of a terminating GaP segment produces the outer shell of GaP (outer shaded region). As a result, an EDXS scan across line 1 will measure the GaP outer sheath only as presented in figure 2(b). An EDXS scan across line 2 will measure the GaP sheath at the NW edges, and a GaP sheath superimposed on the GaAsP core near the NW center, as presented in figure 2(c). Finally, an EDXS scan along line 3 will measure in projection through the thickness the GaP sheath near the NW edges, followed by the GaP/GaAsP/GaP three-layer structure closer to the NW center, and finally the

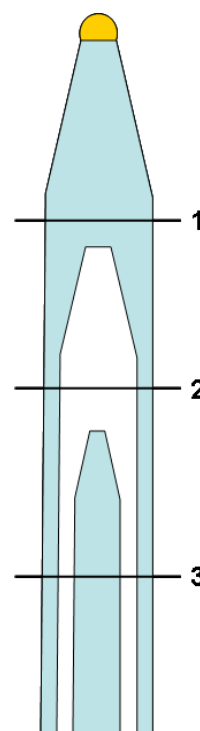

Figure 3. Conceptual drawing of the core–multishell NW structure. The shaded regions illustrate the GaP layers, while the white region is representative of the GaAsP layer. The hemispherical Au particle is evident at the top of the nanowire. The lines labeled 1, 2, and 3 are in positions equivalent to those shown in figure 2(a).

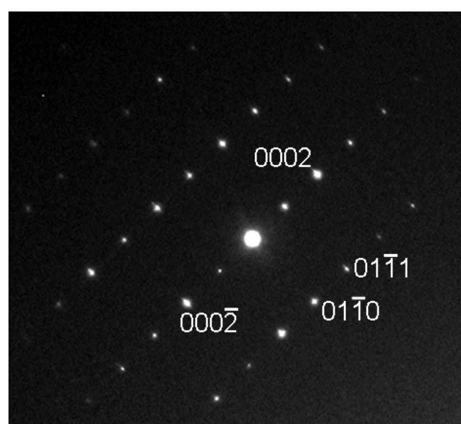

Figure 4. SAD pattern from the middle GaAsP segment of a NW.

entire GaP/GaAsP/GaP/GaAsP/GaP five-layer stack along the NW center.

EDXS point measurements were taken at the center of the GaAsP layer (middle segment) of several NW specimens, to determine the absolute composition within this region. Due to the inhomogeneous arrangement (core–shell structure) of As and P atoms along the radial direction of each NW, a cylindrical approximation method was used to determine the composition of the GaAsP layer alone. In this method, the atomic concentration of phosphorus was measured in a region where the GaAsP core is encapsulated by the GaP shell. Using this information in conjunction with the thickness of the respective layers at the point of the measurement (as determined from the radial EDXS linescans), a thickness weighted average value for the measured composition may be determined according to

$$C_{\mathrm{CS}} D = C_{\mathrm{S}}(D - d) + C_{\mathrm{C}} d \qquad (1)$$

where C_{S}, C_{C} and C_{CS} are the phosphorus atomic concentration values as measured in the GaP shell (50% P), the GaAsP core, and the combined GaP/GaAsP/GaP region, respectively. D is the total thickness of the NW at the point of measurement, and d is the diameter of the GaAsP layer alone at the point of measurement. The compositional variance was calculated to be in the range of $\mathrm{GaAs_{0.79}P_{0.21}}$ to $\mathrm{GaAs_{0.72}P_{0.28}}$ amongst the several NWs that were examined with an error in absolute composition below 5%. A range of group V atomic concentrations among different wires is anticipated due to the competition for growth material in the VLS regime where the metallic nanoparticles are of varying size and distribution.

Next, the crystal structure of the NWs was analyzed. A selected area diffraction (SAD) pattern was obtained in the JEOL 2010F from the middle GaAsP segment of a NW. The resulting SAD pattern in figure 4 indicated a wurtzite crystal structure for the $\langle 2\bar{1}\bar{1}0\rangle$ zone axis and a NW growth direction along $\langle 0001\rangle$. Unlike for the GaAsP region, inspection of the GaP regions near the tip and base of the NW revealed the frequent incidence of stacking faults as demonstrated by the HRTEM image in figure 5 for the base region of a NW. This image, and the corresponding SAD pattern, shown in the inset, revealed a wurtzite crystal structure interrupted periodically with stacking faults. This periodicity in the stacking faults is manifested as the streaking in the SAD pattern in the inset in figure 5.

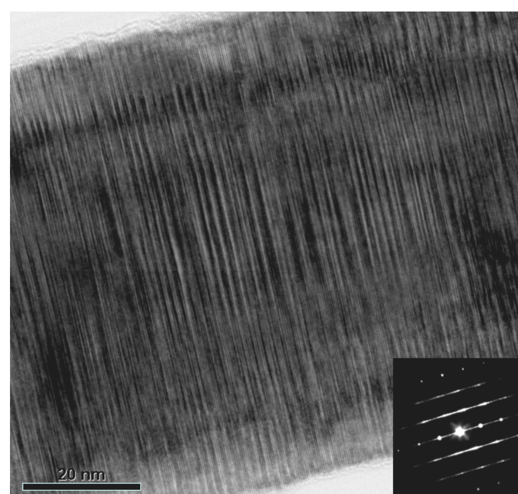

Figure 5. HRTEM image of a region near the NW base revealing the periodicity of stacking faults in the GaP layer. The Au particle (not shown) is towards the top right. The inset shows the corresponding SAD pattern.

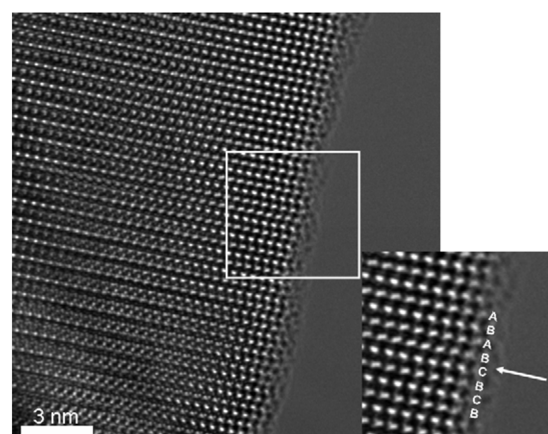

Figure 6. Aberration corrected HRTEM image taken along a NW sidewall. The white rectangle represents the boundaries of the magnified image shown in the inset. The white arrow in the inset points towards a stacking fault corresponding to a change in atomic stacking sequence denoted by the letters A, B, and C. The Au particle (not shown) is towards the top.

To further examine the nature of the stacking faults, the NWs were also examined with the improved resolution of the aberration corrected TEM, as shown in figure 6, for the base region of a NW where three distinct atomic stacking sequences, labeled A, B, and C, are observed. Due to the suppression of the delocalization in the images related to aberration correction, it is possible to directly visualize the interface between the nanowire and vacuum. The images demonstrate the clean surface and the arrangement of the atoms in the outer layers of the nanowire and related surface steps. Predominantly, an ABAB . . . stacking sequence is present, indicative of the wurtzite structure. However, this structure is periodically interrupted by C atomic layers, indicated by an arrow in the inset of figure 6, which is representative of

a stacking fault consisting of a short segment of zincblende structure [19–21]. Further from the surface of the NW, the thickness increases rapidly and the contrast in the image is not directly interpretable, and the changes in stacking sequence are, as a consequence of this, less obvious.

The incidence of stacking faults varied significantly along the length of the NW as indicated by the comparison of the SAD pattern in figure 4 (defect-free GaAsP segment) with the inset of figure 5 (base GaP region with stacking faults). To further illustrate this variation in frequency of stacking faults, we first examine the GaP-to-GaAsP transition close to the base of the NW. Figure 7(a) shows a high angle annular dark-field (HAADF) image of a single NW acquired in the JEOL 2010F, while figure 7(b) shows a bright-field image of the identical NW (the NW top is towards the left). The HAADF image is sensitive to compositional variation, revealing the GaP core region near the base of the NW (right side of figure 7(a)), the GaAsP shell (middle segment of the NW), and the GaP outer shell (left side of figure 7(a)). Elemental As, having higher atomic number than P, appears brighter in the HAADF image. The bright-field image in figure 7(b), on the other hand, is sensitive to the NW structure revealing contrast due to the stacking faults (vertical lines intersecting the NWs). These results reveal that the stacking faults coincide with the GaP base segment of the NW, while the GaAsP middle segment is nearly free of defects.

Next, we examined the GaAsP-to-GaP transition close to the top of the NW. The HAADF and bright-field images shown in figures 7(c) and (d), respectively, reveal a region of GaP that is devoid of stacking faults immediately following the termination of the GaAsP layer. The defects are observed to be reintroduced within the GaP segment after a length of over 200 nm and subsist up to the Au/GaP interface at the NW tip (not shown in figure 7).

We previously reported GaAsP/GaP heterostructure NWs that revealed stacking faults near the top of a long GaAsP segment, while the GaP segment immediately following the GaAsP revealed very few stacking faults. We previously attributed this change in stacking fault density to a compositional dependence of the NW growth mechanisms [17]. However, the present study suggests that NWs are free of stacking faults for a certain growth period following a growth interruption associated with the material transitions. We previously reported similar results for the growth of InP NWs, where an initial wire height of about 300 nm was found free of stacking faults, above which the crystal structure becomes disrupted and the formation of stacking faults becomes frequent [22]. In the present study, it would appear that the segment of GaAsP is shorter than the critical height above which faults are introduced, meaning that the GaAsP remains defect-free. Although not completely understood at present, the regular periodicity of the faults in the defected regions of GaP suggests that their formation is rooted in a dependence upon a cyclical growth process. The growth-interrupted interfaces appear to disrupt this cyclical process resulting in a defect-free region of the NW for a certain growth period. The observation of stacking faults in the base, where there is a layered core–multishell heterostructure, and also in the NW tip, where only a single GaP structure exists, leads us to conclude that the presence of faults does not depend on strain effects induced at lattice-mismatched radial heterointerfaces.

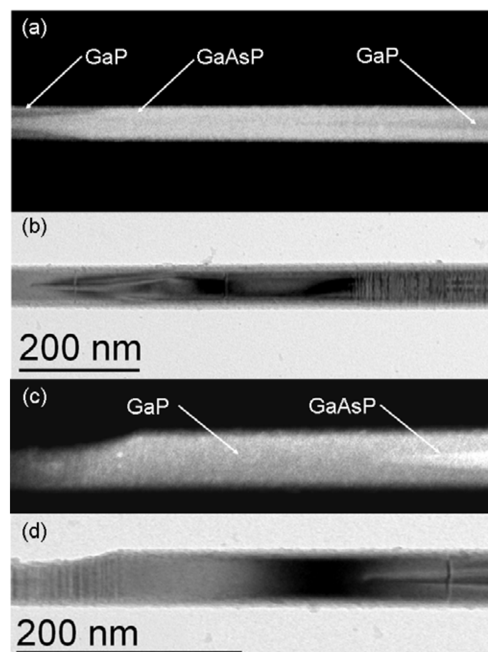

Figure 7. (a) HAADF image of the center region of a NW. The GaP layers (dark regions) are shown to encapsulate the GaAsP layer (bright region). (b) Corresponding bright-field TEM image of the wire shown in (a). The stacking faults evident at the wire base (right-hand side of image) are dramatically reduced with the onset of the GaAsP layer. (c) HAADF image near the NW tip showing the termination of the GaAsP layer within the GaP shell. (d) Corresponding bright-field TEM image of the same NW segment as (c). A defect-free region exists (center of image) following the GaAsP/GaP interface. The stacking faults reappear (left-hand side of image) as the growth continues and persist up to the Au tip. The NW top is towards the left in each image.

4. Conclusions

In summary, GaP/GaAsP/GaP core–multishell heterostructures were monolithically integrated with a Si(111) substrate via GS-MBE according to the VLS growth mechanism. The NWs were of a wurtzite structure and have an aspect ratio of approximately 100. Stacking faults were observed to occur in a periodic fashion along the base and at the tips of the NWs in the GaP regions. The disappearance of faults, coincident with growth interruptions, suggests the potential for MBE growth of defect-free NWs. The passivating effects and quantum confinement arising from these core–shell structures are expected to provide devices, monolithically integrated with Si microelectronics, with enhanced performance and functionality.

Acknowledgments

This work was supported by the Natural Sciences and Engineering Research Council of Canada. We extend our gratitude to the staff of the Center for Emerging Device Technologies and the Canadian Center for Electron Microscopy, in particular to Brad Robinson for the GS-MBE growths and rewarding consultations. Thanks to Nadi Braidy for assistance with analytical microscopy work and some high resolution experiments.

References

[1] Minot E D, Kelkensberg F, van Kouwen M, van Dam J A, Kouwenhoven L P, Zwiller V, Borgstrom M T, Wunnicke O, Verheijen M A and Bakkers E P A M 2007 *Nano Lett.* **7** 367
[2] Huang Y, Duan X and Lieber C M 2005 *Small* **1** 142
[3] Agarwal R, Barrelet C J and Lieber C M 2005 *Nano Lett.* **5** 517
[4] Greytak A B, Barrelet C J, Li Y and Lieber C M 2005 *Appl. Phys. Lett.* **87** 151103
[5] Barrelet C J, Bao J, Loncar M, Park H-G, Capasso F and Lieber C M 2006 *Nano Lett.* **6** 11
[6] Qian F, Gradecak S, Li Y, Wen C-Y and Lieber C M 2005 *Nano Lett.* **5** 2287
[7] Lauhon L J, Gudiksen M S, Wang D and Lieber C M 2002 *Nature* **420** 57
[8] Martensson T, Svensson C P T, Wacaser B A, Larsson M W, Seifert W, Deppert K, Gustafsson A, Wallenberg L R and Samuelson L 2004 *Nano Lett.* **4** 1987
[9] Ihn S-G and Song J-I 2007 *Nano Lett.* **7** 39
[10] Park Y S, Lee S-H, Oh J-E, Park C-M and Kang T-W 2005 *J. Cryst. Growth* **282** 313
[11] Bakkers E P A M, van Dam J A, De Franceschi S, Kouwenhoven L P, Kaiser M, Verheijen M, Wondergem H and Van Der Sluis P 2004 *Nat. Mater.* **3** 769
[12] Roest A L, Verheijen M A, Wunnicke O, Serafin S, Wondergem H and Bakkers E P A M 2006 *Nanotechnology* **17** S271
[13] Zervos M and Feiner L-F 2004 *J. Appl. Phys.* **95** 281
[14] Wagner R S and Ellis W C 1964 *Appl. Phys. Lett.* **4** 89
[15] Dubrovskii V G, Sibirev N V, Cirlin G E, Harmand J C and Ustinov V M 2006 *Phys. Rev.* E **73** 021603
[16] Fan H J, Werner P and Zacharias M 2006 *Small* **2** 700
[17] Chen C, Plante M C, Fradin C and LaPierre R R 2006 *J. Mater. Res.* **21** 2801
[18] Plante M C and LaPierre R R 2004 *J. Cryst. Growth* **286** 394
[19] Koguchi M, Kakibayashi H, Yazawa M, Hiruma K and Katsuyama T 1992 *Japan. J. Appl. Phys.* **31** 2061
[20] Akiyama T, Sano K, Nakamura K and Ito T 2006 *Japan. J. Appl. Phys.* **45** L275
[21] Banerjee R, Bhattacharya A, Genc A and Arora B M 2006 *Phil. Mag. Lett.* **86** 807
[22] Cornet D M, Mazzetti V G M and LaPierre R R 2007 *Appl. Phys. Lett.* **90** 013116